Active Vibration Control on a Smart Composite Structure Using Modal-Shaped Sliding Mode Control

Jonathan Rodriguez, Manuel Collet, Simon Chesné

Journal of Vibration and Acoustics. Received June 30, 2021;
Accepted manuscript posted December 21, 2021. doi:10.1115/1.4053358

Active Vibration Control on a Smart Composite Structure using Modal-Shaped Sliding Mode Control

Jonathan Rodriguez *
PostDoctoral Fellow
Université de Lyon, CNRS INSA-Lyon
LaMCoS UMR5229
F-69621,France
Email: jonathan.rodriguez@ec-lyon.fr

Manuel Collet
Professor
Université de Lyon, ECL
LTDS UMR5513
F-69134 Ecully, France
Email: manuel.collet@ec-lyon.fr

Simon Chesné
Assistant Professor
Université de Lyon, CNRS INSA-Lyon
LaMCoS UMR5229
F-69621,France
Email: simon.chesne@insa-lyon.fr

ABSTRACT

This paper proposes an active modal vibration control method based on a modal sliding mode controller applied to a smart material composite structure with integrated piezoelectric transducers as actuators and sensors. First, the electromechanical coupled system is identified using a modal reduced-order model. The sliding surface is based on the modal-filtered states and designed using a general formulation allowing the control of multiple vibration modes with multiple piezoelectric sensors and actuators. The performance and stability of the nonlinear controller are addressed and confirmed with the experimental results on a composite

* Address all correspondence to this author.

smart spoiler-shaped structure. The nonlinear switching control signal, based on the modal-shaped sliding surface improves the performances of the linear part of the control while maintaining not only stability but also robustness. The attenuation level achieved on the target modes on all piezoelectric sensors starts from -14dB up to -22dB, illustrating the strong potential of nonlinear switching control methods in active vibration control.

1 INTRODUCTION

Smart materials have shown great potential in many research and industrial applications. They consist of mechanical structures where actuators and sensors are integrated and enable the global system to interact with its environment, reacting to the experienced strain or stress for instance, and modifying their mechanical properties to counter-act disturbances or achieve any defined actuation objective using a proper control system.

Metallic but also composite smart structures with bonded or integrated piezoelectric transducers have seen their popularity grow in the last decade. As piezoelectric patches are thin, lightweight, and somehow flexible compared to more classical actuation methods, they can adapt to complex shapes and curved surfaces like structural composite elements. Besides, a more distributed actuation can be achieved by multiplying the transducers in the structure as a network manner.

These composite materials have opened up new possibilities in terms of applications like structural health monitoring [1], vibration control [2], and energy harvesting [3].

For active vibration control of smart structures, the challenge is in the design of efficient and robust controllers, whether the objective is broadband vibration control, disturbance rejection, or modal control [4]. Since real industrial smart structures are complex systems, sometimes too complex to be modeled precisely and subject to parametric uncertainties, robustness is a key property when designing active vibration controllers.

Many different linear control methods have been investigated and applied to active vibration control of smart structures with piezoelectric transducers: velocity or force/acceleration feedback, optimal control [5], or robust control [6] among others. These methods remain linear with the induced limitations in stability and robustness that it entails. Thus, optimal tuning always resides in a trade-off between control performance and robustness to uncertainties.

To push further these limitations and improve active vibration control performance and especially robustness, nonlinear control methods have received more and more attention in recent years. One of them is sliding mode control (SMC) which has been widely used for tracking control problems in robotics typically [7]. The idea behind this method is to define a sliding surface, being a linear or nonlinear function of the error vector, and then apply a discontinuous switching control signal based on the position of the system in the phase plane with respect to the sliding surface. Thus,

the closed-loop dynamics are reduced to those of the sliding variable and forced to converge to the sliding manifold. Many different SMC controllers have been investigated but few are applied to vibration control problems and even fewer to smart structures. Lots of applications of SMC control in vibration problems are reduced to low-frequency dynamics and tracking problems, typically vehicle active suspensions systems [8–11]. Hu and Friswell [12] applied an SMC for vibration control of a flexible spacecraft. However, the switching control was only applied for attitude control while the vibration problem was handled by a linear modal velocity feedback control signal. Much more recently, Concha A et al. [13] developed an SMC for an active tuned mass damper (ATMD) on a building subject to seismic vibrations. The proposed controller was compared to classical LQG control and also optimal SMC where the switching function is designed using optimal control theory.

Focusing on vibration control for smart structures with piezoelectric transducers, the majority of the investigation has been to propose new sliding surfaces based on modal models [20, 21], SMC observers [22], sometimes associated with adaptive strategies [23] or fuzzy logic [24, 25]. However, the proposed controllers are in general only experimented on academic systems like cantilever beams, structures lacking representativity regarding industrial applications. In addition, robustness properties, yet essential for real and complex applications, are rarely considered. For instance, Hu and Zhu in [26] propose also a sliding mode controller for vibration control of a beam with piezoelectric transducers. However, only the linear part of the SMC method is used to control the vibrations of the considered smart structure. Thus losing the robustness benefit theoretically provided by the nonlinear switching part of SMC.

To be able to focus control energy on a particular bandwidth or mode, frequency shaping method [27] has also been investigated within the SMC formulation, beginning with Young and Özgüner [14]. The main idea is to define an augmented plant with the states of the system and those of a dynamic sliding surface being a linear operator of the error vector [15–18]. Zuo and Slotine in [19] developed a frequency-shaped SMC for modal control of an isolation table, targeting with the appropriate dynamic sliding surface a skyhook effect for the lower frequency modes. Besides, the SMC was also enhanced with an adaptive observer to identify online the modal parameters of the system.

The contribution of this paper relies upon the proposition of a complete multi-modal vibration controller based on SMC using multiple sensors and actuators. The proposed approach especially fits with smart material structures with networks of piezoelectric transducers. The modal-shaped sliding surface allows the switching control part to focus the control energy only on the targeted modes, thus improving significantly the performance and robustness of the linear part of the control. Also, the designed controller is applied to a composite smart spoiler-shaped structure, representative of potential real applications especially in transportation where independent self-sensing and self-controlling structural parts have a great perspective. It is worth noticing that the real system presents largely noisy signals since the lack of knowledge does not allow us to determine a precise electromechanical model. Thus, the composite smart structure is

Journal of Vibration and Acoustics. Received June 30, 2021;
Accepted manuscript posted December 21, 2021. doi:10.1115/1.4053358

also a good candidate to emphasize the need for a robust controller.

This paper is organized as follows. The next section 2 presents the development of the general formulation of the modal state-space realization of the composite smart structure. Then, the procedure describing the design of the modal-shaped sliding mode controller is developed in detail in section 3. Finally, in section 4 are presented all the results of the modal identification method, the numerical parameters of the controller, and the experimental results.

2 SYSTEM IDENTIFICATION

The experimental system considered in this manuscript is a smart composite structure with N_a PZT actuators and N_s PZT sensors. For the modeling process, n vibration modes are selected to be observed and controlled, within the desired bandwidth, and supposedly sufficiently separated to consider every contribution of modes $j \neq i$ negligible at the modal characteristic frequency ω_i.

Besides, the transfer function between actuator l and sensor k can be estimated by a sum of n second order systems:

$$H_{k,l}(s) = \sum_{i}^{n} \frac{M_i^{k,l} e^{j\phi_i^{k,l}}}{s^2 + 2\xi_i\omega_i s + \omega_i^2} \tag{1}$$

where $s = j\omega$ is the Laplace variable, ω_i is the mode frequency and ξ_i the modal damping ratio. $M_i^{k,l}$ and $\phi_i^{k,l}$ are respectively the modal magnitude and phase from i^{th} mode. All the modal parameters are estimated using the rational fraction form (RFP) [28, 29] from the measured transfer function $H_{k,l}^{exp}(\omega)$.

Nevertheless, the expression (1) does not have a state space realization with real matrices (A, B, C, D). For instance in [30], the coefficients $M_i^{k,l} e^{j\phi_i^{k,l}}$ are replaced with appropriate time delays, while keeping the amplitudes $M_i^{k,l}$ within the observation matrix C. Thus, the transfer function $H_{k,l}(s)$ is modified to fit with a polynomial rational transfer function:

$$H_{k,l}^{ident}(s) = \sum_{i}^{n} \frac{a_i^{k,l} + b_i^{k,l} s}{s^2 + 2\xi_i\omega_i s + \omega_i^2} \tag{2}$$

where $(a_i^{k,l}, b_i^{k,l}) \in \mathbb{R}^2$ and:

$$\begin{aligned} a_i^{k,l} &= Re(M_i^{k,l} e^{j\phi_i^{k,l}}) \\ b_i^{k,l} &= Im(M_i^{k,l} e^{j\phi_i^{k,l}}) \frac{1}{\omega_i} \end{aligned} \tag{3}$$

A state-space realization of subsystem G_l is now defined to characterize the transfer function vector between the voltage input of the l^{th} PZT actuator $u_l \in \mathbb{R}$ and the voltage response vector $y_l \in \mathbb{R}^{N_s}$ of the PZT sensors due to u_l:

$$G_l \begin{cases} \dot{x}_l = A_l x_l + B_l u_l \\ y_l = C_l x_l \end{cases} \tag{4}$$

with $A_l \in \mathbb{R}^{2n \times 2n}$, $B_l \in \mathbb{R}^{2n}$, $C_l \in \mathbb{R}^{N_s \times 2n}$, $x_l = [q_l, \dot{q}_l]^T$, $q_l \in \mathbb{R}^n$ and $\dot{q}_l \in \mathbb{R}^n$ as the modal state and its time derivative respectively.

From (2) and (4), the matrices A_l,B_l and C_l are then expressed in the following form:

$$A_l = \begin{bmatrix} 0_n & I_n \\ -diag(\omega_i^2) & -2diag(\xi_i \omega_i) \end{bmatrix}_{2n,2n} \tag{5}$$

$$B_l = \begin{bmatrix} 0_{n,1} \\ B_1^l \\ \vdots \\ B_n^l \end{bmatrix}_{2n,1} \tag{6}$$

$$C_l = \begin{bmatrix} C_1^1 & \cdots & C_n^1 & 0_{1,n} \\ \vdots & \ddots & \vdots & 0_{1,n} \\ C_1^{N_s} & \cdots & C_n^{N_s} & 0_{1,n} \end{bmatrix}_{N_s,2n} \tag{7}$$

Journal of Vibration and Acoustics. Received June 30, 2021;
Accepted manuscript posted December 21, 2021. doi:10.1115/1.4053358

The transfer function vector $G_l(s) \in \mathbb{C}^{N_s}$ from system (4) such that $Y_l(s) = G_l(s)U_l(s)$ is:

$$G_l(s) = C_l \left(sI_{2n} - A_l\right)^{-1} B_l \tag{8}$$

From (2) and (8), it comes the following identification:

$$a_i^{k,l} + j\omega_i b_i^{k,l} = C_i^k B_i^l \tag{9}$$

When considering electromechanical systems, the independent identification of the coefficients C_i^k and B_i^l from a generalized model can be particularly difficult and inaccurate for weakly coupled structures. Since only the products $C_i^k B_i^l$ are necessary to design the controller, the need for a more complex identification process to compute separately the coefficients is avoided. Thus, it can be written the following definitions for the matrices B_l and C_l where a choice is made to force the terms B_i^l to 1:

$$\begin{aligned} B_l &= [0_{1,n}\ 1_{1,n}]^T \\ C_l &= \begin{bmatrix} a_1^{1,l} & \cdots & a_n^{1,l} & b_1^{1,l} & \cdots & b_n^{1,l} \\ \vdots & \ddots & \vdots & \vdots & \ddots & \vdots \\ a_1^{N_s,l} & \cdots & a_n^{N_s,l} & b_1^{N_s,l} & \cdots & b_n^{N_s,l} \end{bmatrix} \end{aligned} \tag{10}$$

Finally, the total system $G(s)$ summing the effects of each actuator on the N_a sensors such that:

$$\begin{aligned} Y(s) &= \sum_{l=1}^{N_a} Y_l(s) \\ &= \sum_{l=1}^{N_a} G_l(s)U_l(s) \\ &= G(s)U(s) \end{aligned} \tag{11}$$

with $U(s) = [U_1(s) \ \cdots \ U_{Na}(s)]^T$ is defined with the following state-space realization:

$$G \begin{cases} \dot{x}' = A'x' + B'u \\ y = C'x' \end{cases} \tag{12}$$

where $x' = [x_1^T \ \cdots \ x_{Na}^T]^T$,$u = [u_1 \ \cdots \ u_{Na}]^T$ and $y = \sum_{l=1}^{Na} y_l$. The matrices $A' \in \mathbb{R}^{2n.N_a \times 2n.N_a}$, $B' \in \mathbb{R}^{2n.N_a \times N_a}$, and $C' \in \mathbb{R}^{N_s \times 2n.N_a}$ are defined as :

$$A' = \begin{bmatrix} A_1 & 0_{2n} & \cdots & 0_{2n} \\ 0_{2n} & A_2 & \cdots & 0_{2n} \\ \vdots & \vdots & \ddots & \vdots \\ 0_{2n} & 0_{2n} & \cdots & A_{N_a} \end{bmatrix} \tag{13}$$

$$B' = \begin{bmatrix} B_1 & 0_{2n,1} & \cdots & 0_{2n,1} \\ 0_{2n,1} & B_2 & \cdots & 0_{2n,1} \\ \vdots & \vdots & \ddots & 0_{2n,1} \\ 0_{2n,1} & 0_{2n,1} & \cdots & B_{N_a} \end{bmatrix} \tag{14}$$

$$C' = \begin{bmatrix} C_1 & C_2 & \cdots & C_{Na} \end{bmatrix} \tag{15}$$

However, this state-space realization is poorly balanced in terms of observability and controllability. The matrix B' only contains unitary values while the observation matrix C' is filled with the coefficients $a_i^{k,l}$, of the same order of magnitude than ω_i, and making the system much more observable than controllable. Hence, using the Gramian method [31], a transformation is applied to the states such that $T \in \mathbb{R}^{2n.N_a \times 2n.N_a}$. Thus, the new state vector is $x = T^{-1}x'$ and the new balanced state-space realization of G is:

$$G \begin{cases} \dot{x} = Ax + Bu \\ y = Cx \end{cases} \tag{16}$$

Journal of Vibration and Acoustics. Received June 30, 2021;
Accepted manuscript posted December 21, 2021. doi:10.1115/1.4053358

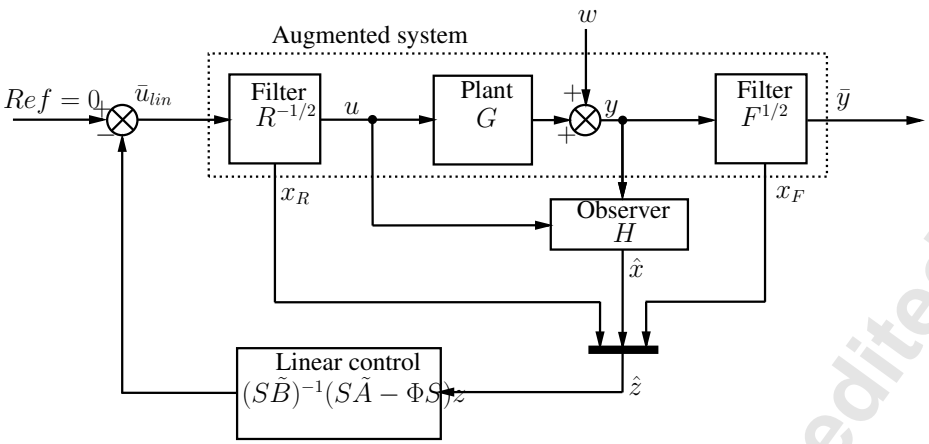

Fig. 1: Linear closed-loop system with augmented plant and observer.

with $A = T^{-1}A'T$, $B = T^{-1}B'$ and $C = C'T$.

3 SLIDING MODE CONTROL DESIGN

In this section, a modal-shaped sliding mode control is designed with both linear and nonlinear terms. The complete controller stability is also addressed using the Popov frequency criterion for closed-loops with nonlinear memoryless feedback.

3.1 Augmented modal-shaped plant

The controller design is based on sliding mode control theory [7]. Nevertheless, the objective is to concentrate the control energy on the n targeted modes.

To achieve this objective, one has to design first two stable filters $R^{-1/2}$ and $F^{1/2}$, respectively proper and strictly proper. They are applied as pre- and post-filters to the identified plant $G(s)$ such as in Figure 1. Their state-space realizations are expressed by:

$$R^{-1/2}(s) = \begin{cases} \dot{x}_R = A_R x_R + B_R \bar{u} \\ u \ = C_R x_R \end{cases} \tag{17}$$

Journal of Vibration and Acoustics. Received June 30, 2021;
Accepted manuscript posted December 21, 2021. doi:10.1115/1.4053358

$$F^{1/2}(s) = \begin{cases} \dot{x}_F = A_F x_F + B_F y \\ \bar{y} \ = C_F x_F + D_F y \end{cases} \tag{18}$$

Thus, an augmented system, containing the modal-shaped filters is defined with a new state vector $z = [x^T \, x_F^T \, x_R^T]^T$ such that:

$$\begin{cases} \begin{bmatrix} \dot{x} \\ \dot{x_F} \\ \dot{x_R} \end{bmatrix} = \begin{bmatrix} A & 0 & BC_R \\ B_F C & A_F & 0 \\ 0 & 0 & A_R \end{bmatrix} \begin{bmatrix} x \\ x_F \\ x_R \end{bmatrix} + \begin{bmatrix} 0 \\ 0 \\ B_R \end{bmatrix} \bar{u} \\ \\ \bar{y} \ = [D_F C \ C_F \ 0] \begin{bmatrix} x \\ x_F \\ x_R \end{bmatrix} \end{cases} \tag{19}$$

where $\bar{u} \in \mathbb{R}^{N_a}$ and $\bar{y} \in \mathbb{R}^{N_s}$ are the new system input and output. The state space (19) can be expressed more easily by:

$$\begin{cases} \dot{z} = \tilde{A} z + \tilde{B} \bar{u} \\ \bar{y} = \tilde{C} z \end{cases} \tag{20}$$

with $\tilde{A} \in \mathbb{R}^{N \times N}$, $N \geq n + 2$, $\tilde{B} \in \mathbb{R}^{N \times N_a}$, $\tilde{C} \in \mathbb{R}^{N_s \times N}$.

3.2 Equivalent control

A switching function $\sigma \in \mathbb{R}^{N_a}$ such that $\sigma = Sz$ with $S \in \mathbb{R}^{N_a \times N}$ must be designed to guarantee the system convergence to the real sliding mode $||\sigma|| \leq \epsilon$.

Supposing an ideal sliding mode motion *i.e* $\sigma = \dot{\sigma} = 0_{N_a}$, from (20) we can write:

$$S\dot{z} = S\tilde{A}z + S\tilde{B}\bar{u} = 0 \tag{21}$$

The equivalent control $\bar{u}_{eq}$, representing the control action required to maintain the system states on the switching surface is then:

$$\bar{u}_{eq} = -(S\tilde{B})^{-1}S\tilde{A}z \tag{22}$$

where $(S\tilde{B})$ being non singular is a constraint in the design of the switching function S and will be addressed in the next subsection.

3.3 Switching function design

A coordinate transformation is now introduced to the state z to obtain a regular form state space representation of (20). This step is necessary since the existence of $(S\tilde{B})^{-1}$ in (22) needs to be guaranteed. Assuming $rank(\tilde{B}) = N_a$, there exists an orthogonal matrix $T_r \in \mathbb{R}^{N\times N}$ such that:

$$T_r\tilde{B} = \begin{bmatrix} 0 \\ B_2 \end{bmatrix} \tag{23}$$

where $B_2 \in \mathbb{R}^{N_a\times N_a}$ is non-singular. In practice, such matrix can be obtained from QR factorization of $\tilde{B}$, *i.e* :

$$\begin{aligned} \tilde{B} &= \Psi\Lambda \\ &= [\Psi_1 \;\; \Psi_2] \begin{bmatrix} \Lambda_1 \\ 0 \end{bmatrix} \end{aligned} \tag{24}$$

with $\Lambda_1 \in \mathbb{R}^{N_a \times N_a}$ non-singular and upper-triangular. It comes:

$$T_r = [\Psi_2 \;\; \Psi_1]^{-1} \tag{25}$$

Let $\bar{z} = T_r z$ and partition the new state vector such that:

$$\bar{z} = \begin{bmatrix} z_1 \\ z_2 \end{bmatrix} \tag{26}$$

where $z_1 \in \mathbb{R}^{N-N_a}$ and $z_2 \in \mathbb{R}^{N_a}$. The linear system $(\tilde{A}, \tilde{B})$ becomes in the $\bar{z}$ coordinates:

$$\begin{cases} \dot{z_1} = A_{11} z_1 + A_{12} z_2 \\ \dot{z_2} = A_{21} z_1 + A_{22} z_2 + B_2 u \end{cases} \tag{27}$$

in which:

$$T_r A T_r^T = \begin{bmatrix} A_{11} & A_{12} \\ A_{21} & A_{22} \end{bmatrix} \tag{28}$$

The switching function in the $\bar{z}$ coordinate system is:

$$S T_r^T = [S_1 \;\; S_2] \tag{29}$$

with $S_1 \in \mathbb{R}^{N_a \times (N-N_a)}$ and $S_2 \in \mathbb{R}^{N_a \times N_a}$. From (23) and (29), it comes $S\tilde{B} = S_2 B_2$. Therefore, defining S_2 such that $det(S_2) \neq 0$ guarantees the existence of $(S\tilde{B})^{-1}$.

Thus, when the sliding mode occurs for (27) *i.e.* $Sz = 0$, we can write:

$$Sz = S_1 z_1 + S_2 z_2 = 0 \tag{30}$$

$$z_2 = -M z_1 \tag{31}$$

with $M = S_2^{-1} S_1$. Substituting in (27) gives:

$$\dot{z}_1 = (A_{11} - A_{12} M)\, z_1 \tag{32}$$

From (29), it comes also the switching function form:

$$S = S_2 [M \;\; I_{N_a}] T_r \tag{33}$$

A common choice for S_2 is $S_2 = B_2^{-1}$ which implies $(S\tilde{B}) = I_{N_a}$. Meanwhile, the matrix M is defined using linear quadratic minimization from (32). We define a positive definite weight matrix $Q \in \mathbb{R}^{N \times N}$ and the performance index J to minimize:

$$J = \frac{1}{2} \int_{t_s}^{+\infty} z^T Q z \, dt \tag{34}$$

where t_s is the time at which the sliding mode occurs. The matrix Q is transformed and partitioned in the $\bar{z}$ coordinate system:

$$T_r Q T_r^T = \begin{bmatrix} Q_{11} \; Q_{12} \\ Q_{12}^T \; Q_{22} \end{bmatrix} \tag{35}$$

As developed in [7], by choosing an appropriate virtual control vector $v = z_2 + Q_{22}^{-1} Q_{12}^T z_1$, the performance

index can be re-written into:

$$J = \frac{1}{2}\int_{t_s}^{+\infty} z_1^T \hat{Q} z_1 + v^T Q_{22} v \; dt \tag{36}$$

Then, to determine the matrix M, the virtual control v is substituted into $\dot{z}_1$ expression from (27) leading to the next linear system:

$$\dot{z}_1 = \hat{A} z_1 + A_{12} v \tag{37}$$

with $\hat{Q} = Q_{11} - Q_{12}Q_{22}^{-1}Q_{12}^T$ and $\hat{A} = A_{11} - A_{12}Q_{22}^{-1}Q_{12}^T$. Finally, M is solution to the LQ problem $(\hat{A}, A_{12}, \hat{Q}, Q_{22})$.

3.4 Linear system stability

Since the dynamics of the closed-loop system are reduced to those of the sliding vector σ, let us define a candidate Lyapunov function $V(\sigma)$ to design the final control and guarantee the convergence of σ to a considered small vicinity of the sliding surface:

$$V = \sigma^T P \sigma \tag{38}$$

with $P \in \mathbb{R}^{m,m}$ a chosen positive definite and diagonal matrix satisfying the Lyapunov equation $P\Phi + \Phi^T P = -I$. From this equation comes the stable matrix Φ used to complete the equivalent control with a stabilizing control part defined by $\bar{u}_{stab} = (S\tilde{B})^{-1}\Phi S z$ since $\bar{u}_{eq}$ only gives a marginally stable closed-loop.

Then, the linear control $\bar{u}_{lin}$ is defined as:

$$\bar{u}_{lin} = \bar{u}_{eq} + \bar{u}_{stab} \tag{39}$$

$$= -(S\tilde{B})^{-1} S\tilde{A} z + (S\tilde{B})^{-1}\Phi S z \tag{40}$$

$$= -(S\tilde{B})^{-1}\left(S\tilde{A} - \Phi S\right) z \tag{41}$$

Journal of Vibration and Acoustics. Received June 30, 2021;
Accepted manuscript posted December 21, 2021. doi:10.1115/1.4053358

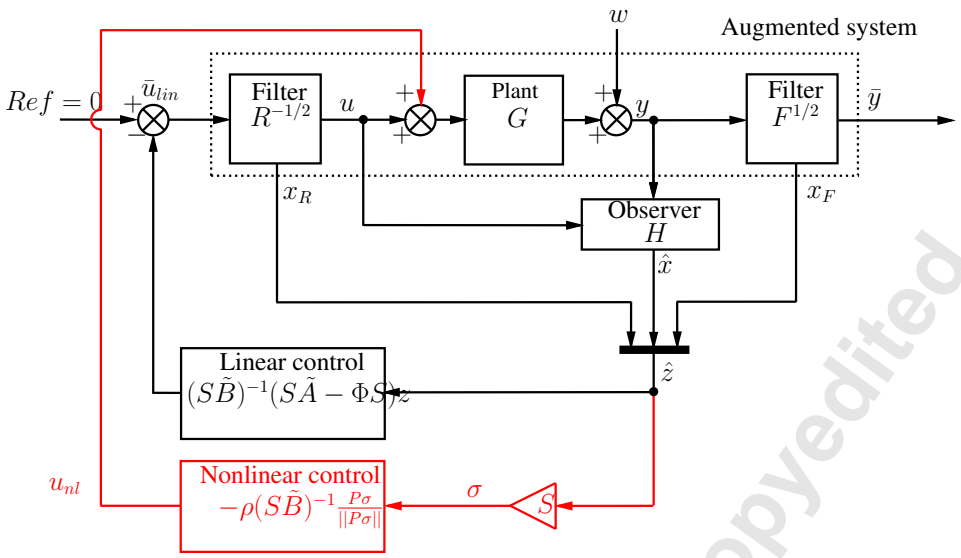

Fig. 2: Linear and nonlinear closed-loop for switching control.

Thus, it comes:

$$\begin{aligned}
\dot{V} &= \sigma^T P\dot{\sigma} + \dot{\sigma}^T P\sigma \\
&= z^T S^T P\left(S\tilde{A}z + S\tilde{B}\bar{u}\right) + \left(S\tilde{A}z + S\tilde{B}\bar{u}\right)^T PSz \\
&= z^T S^T \Phi^T PSz + z^T S^T P\Phi Sz \\
&= \sigma^T\left(\Phi^T P + P\Phi\right)\sigma \\
&= -\sigma^T\sigma \leq 0
\end{aligned} \tag{42}$$

which guarantees the closed-loop stability of the linear control. □

3.5 Nonlinear control component and absolute stability

The main advantage of SMC is the use of the sliding vector σ to design a switching control term forcing its dynamics to reach faster the sliding mode condition $\sigma = \dot{\sigma} = 0$. Thus, using the switching function S, a nonlinear

control part u_{nl} is designed such that:

$$u_{nl} = -\rho(S\tilde{B})^{-1}\frac{P\sigma}{||P\sigma||} \tag{43}$$

with $\rho \in \mathbb{R}^+$ and $\frac{P\sigma}{||P\sigma||}$ equivalent to a vector sign function. As it is not desirable to pre-filter the switching control signal with $R^{-1/2}$, u_{nl} is directly applied to the real system G as in Figure 2.

Then, the total control can be expressed with the following expression:

$$\begin{aligned}\bar{u} &= \bar{u}_{lin} + \bar{u}_{nl} \\ &= -(S\tilde{B})^{-1}\left(S\tilde{A} - \Phi S\right)z \\ &\quad -R^{1/2}\left\{\rho(S\tilde{B})^{-1}\frac{P\sigma}{||P\sigma||}\right\}\end{aligned} \tag{44}$$

where $R^{1/2}\{\cdot\}$ represents the inverse transfer function of pre-filter $R^{-1/2}$. Thus, the new dynamics of the reduced closed-loop system are:

$$\begin{aligned}\dot{\sigma} &= S\tilde{A}z + S\tilde{B}\bar{u} \\ &= \Phi\sigma - \rho(S\tilde{B})^{-1}R^{1/2}\left\{\frac{P\sigma}{||P\sigma||}\right\}\end{aligned} \tag{45}$$

This closed-loop is equivalent to the so-called Lurie control problem in nonlinear control where a linear system has a nonlinear memoryless feedback component as in figure 3. The expression (45) can be re-written as:

$$\begin{aligned}\sigma(s) &= \rho\left(sI - \Phi\right)^{-1}(S\tilde{B})^{-1}R^{1/2}(s)\mathcal{L}\left\{-\frac{P\sigma}{||P\sigma||}\right\} \\ &= -K(s)\mathcal{L}\left\{f(\sigma)\right\}\end{aligned} \tag{46}$$

where $\mathcal{L}(\cdot)$ is the Laplace transformation. The nonlinear function $f(\sigma) = \frac{P\sigma}{||P\sigma||}$ belongs to the sector $[0, 1/\epsilon]$ with $\epsilon << 1$ since for practical concerns, the discontinuous portion of the control signal is approximated by $\frac{P\sigma}{||P\sigma||} \approx$

$\frac{P\sigma}{||P\sigma||+\epsilon}$.

Thus, using the Popov's absolute stability criterion [32], a sufficient condition for the closed-loop (46) to be stable is if $\exists\, q \in \mathbb{R}$ s.t:

$$Re\left(K(j\omega)\right) - q\omega Im\left(K(j\omega)\right) + \epsilon > 0 \tag{47}$$

One has to define first the function $K(s) \in \mathbb{C}^{Na\times Na}$. For the sake of simplicity, the matrix Φ is defined diagonal symmetric with eigenvalues $\lambda_m \in \mathbb{R}^-$. Then the diagonal transfer function matrix associated with the matrix Φ is of the form:

$$(sI - \Phi)^{-1} = diag\left\{\frac{1}{s-\lambda_m}\right\} \tag{48}$$

with $m \in [1; N_a]$. The filter $R^{-1/2}$ is defined as a second order low pass filter:

$$R^{-1/2}(s) = I_{Na} \times \frac{\alpha}{1 + s^2/\omega_{LP}^2 + s/(Q_f\omega_{LP})} \tag{49}$$

where $\alpha \in \mathbb{R}^+$, $\omega_{LP} \in \mathbb{R}^+$ and $Q_f \in \mathbb{R}^+$ are chosen positive real parameters.

Then, the function $K(\omega)$ identified in (46) has the following form:

$$K(\omega) = \rho(S\tilde{B})^{-1} \times \frac{(-\lambda_m - j\omega)(1 - \omega^2/\omega_{LP}^2 + j\omega/(Q_f\omega_{LP}))}{\alpha(\omega^2 + \lambda_m^2)} \tag{50}$$

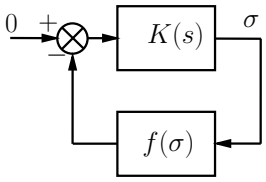

Fig. 3: Reduced dynamics of the system for absolute stability.

Substituting (50) into (47) and considering $\epsilon \approx 0$ gives the following sufficient condition for absolute stability:

$$-\lambda_m + \frac{\lambda_m \omega^2}{\omega_{LP}^2} + \frac{\omega^2}{Q_f \omega_{LP}} - q\omega^2 \left(\frac{-\lambda_m}{Q_f \omega_{LP}} + \frac{\omega^2}{\omega_{LP}^2} - 1 \right) > 0 \tag{51}$$

By considering the case $q = 0$, equation (51) requires $K(s)$ to fulfill the principle of passivity *i.e.* being strictly positive real such that:

$$\begin{aligned} Re\left(K(j\omega)\right) &> 0 \\ -\lambda_m + \frac{\lambda_m \omega^2}{\omega_{LP}^2} + \frac{\omega^2}{Q_f \omega_{LP}} &> 0 \end{aligned} \tag{52}$$

In practice, it is always possible to design a filter $R^{-1/2}$ of the form (49) satisfying the sufficient condition (52) and thus garanteeing absolute stability of the nonlinear reduced dynamics σ. □

3.6 Observation

Since the full-state feedback is necessary to compute the control signal $\bar{u}$, a Kalman filter is designed to estimate only the state x from y since it is not necessary to estimate the states of $R^{-1/2}$ and $F^{1/2}$:

$$\dot{\hat{x}} = A\hat{x} + Bu + L\left(y - C\hat{x}\right) \tag{53}$$

where $\hat{x} \in \mathbb{R}^{2n}$ is the state estimation. The observer gain matrix L is designed considering a low level of co-variance from measurement noise and state perturbation. Finally the new state $\hat{z}$ with the linear and nonlinear control terms are defined as:

Journal of Vibration and Acoustics. Received June 30, 2021;
Accepted manuscript posted December 21, 2021. doi:10.1115/1.4053358

$$\begin{cases} \hat{z} & = [\hat{x}^T \;\; x_F^T \;\; x_R^T]^T \\ \sigma & = S\hat{z} \\ \bar{u}_{lin} & = -(S\tilde{B})^{-1}\left(S\tilde{A} - \Phi S\right)\hat{z} \\ u_{nl} & = -\rho(S\tilde{B})^{-1}\frac{P\sigma}{||P\sigma||} \end{cases} \tag{54}$$

4 EXPERIMENTAL APPLICATION TO A COMPOSITE SMART STRUCTURE

In the following section, the proposed modal sliding mode controller is applied to a smart composite structure with integrated PZT transducers as excitation, in-loop sensors, and actuators. In addition to the identification process and the resulting controller synthesis, a robustness analysis is performed where uncertainties on the identified modal phases are introduced in the observer computation, or the linear control mistuned to set the closed-loop unstable on purpose. The resulting simulations of such degraded controllers on the ideally identified system are aimed to support and illustrate the robustness of the proposed identification and nonlinear control approach. Finally, the controller is applied gradually to the physical system, beginning with only the linear part $\bar{u}_{lin}$, then only the switching control u_{nl}, and finally the complete SMC.

4.1 Experimental setup

The physical structure supporting the experimental part is a composite spoiler profile manufactured by the M3M Laborator (UTBM, France) with a 3 layers architecture. Two glass fiber layers enclose an active layer containing 6 PZT transducers of 25 mm diameter and 150μm thickness. The transducers are aligned and separated in the horizontal plane by a distance of 50mm (center to center). The spoiler has the following dimensions: $1150 \times 300 \times 25$ mm as shown in the Figures 4 and 5.

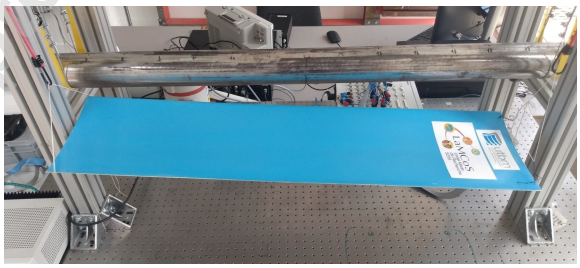

Fig. 4: Smart composite structure : global view.

Journal of Vibration and Acoustics. Received June 30, 2021;
Accepted manuscript posted December 21, 2021. doi:10.1115/1.4053358

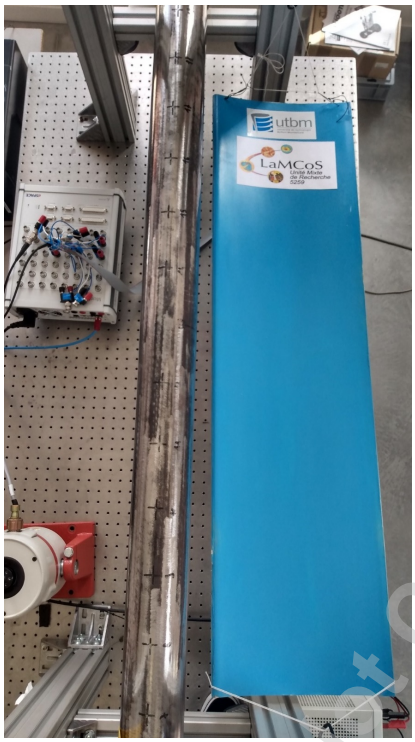

Fig. 5: Smart composite structure : top view.

The system is represented schematically on Figure 6 with the 6 PZT transducers and the connections to the Dspace MicroLabBox controller with the computer. The composite smart structure is isolated from the ground using low stiffness elastic components.

4.2 Identification results

For the identification process, a white noise signal of maximum amplitude 3V and 20s length is sent to the PZT actuators 1 and 6 sequentially with a sample frequency of 20kHz. The measured frequency response functions (FRF) are shown in the Figures 7 and 8 where 3 modes to be controlled are selected: 770Hz, 1282Hz, and 1576Hz. The choice of the bandwidth of interest between 500Hz and 2000Hz has been made considering potential acoustic applications. In addition, PZT transducers in general offer poor control authority at low frequencies since their strain is quite limited.

Finally, a synthesis of the identification results is presented in Table 1 where the modal parameters ω_i and ξ_i are arbitrarily taken from $H_{2,1}(s)$ due to slight variations from one FRF to another.

The measured FRF's from actuators to sensors are displayed in the Figures 9, 10, and 11 for the transducers 2,3, and 5 respectively. At the vicinity of the target modes, the modal response reconstruction method gives the correct magnitude and phase.

Journal of Vibration and Acoustics. Received June 30, 2021;
Accepted manuscript posted December 21, 2021. doi:10.1115/1.4053358

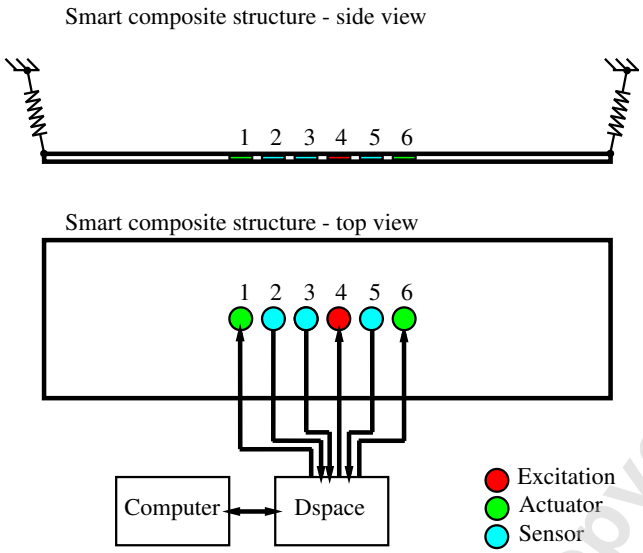

Fig. 6: Schematic representation of the experiment.

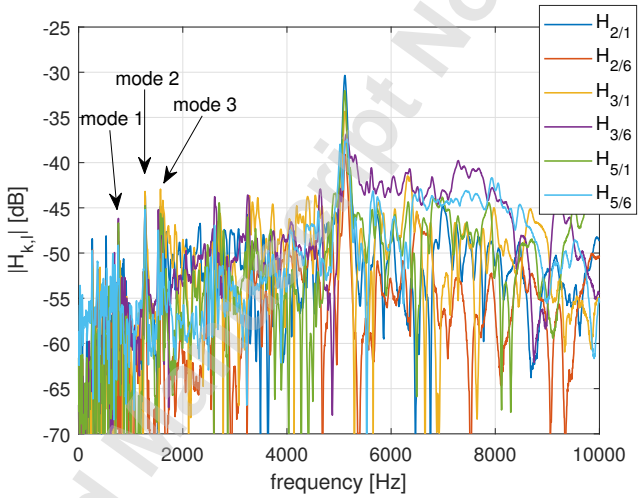

Fig. 7: FRF's of PZT sensors 2,3, and 5 to actuation (PZT 1 and 6), targeted modes for control

4.3 Control parameters

The pre- and post- filters $F^{1/2}$ and $R^{-1/2}$ are determined to emphasize the control effort on the chosen modes by shaping the sliding surface σ. As already defined in (49), $R^{-1/2}(s)$ is a 2^{nd} order low pass filter with $Q_f = 1$ and $\omega_{LP} = \omega_3$. On the other hand, the post-filter $F^{1/2}(s)$ is the product of a sum of modal filters around the target modes

Journal of Vibration and Acoustics. Received June 30, 2021;
Accepted manuscript posted December 21, 2021. doi:10.1115/1.4053358

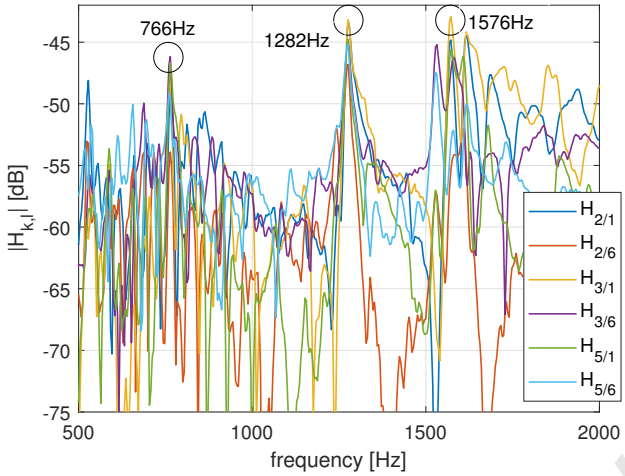

Fig. 8: FRF's of PZT sensors 2,3, and 5 to actuation (PZT 1 and 6), targeted modes for control with zoom on the bandwidth of interest.

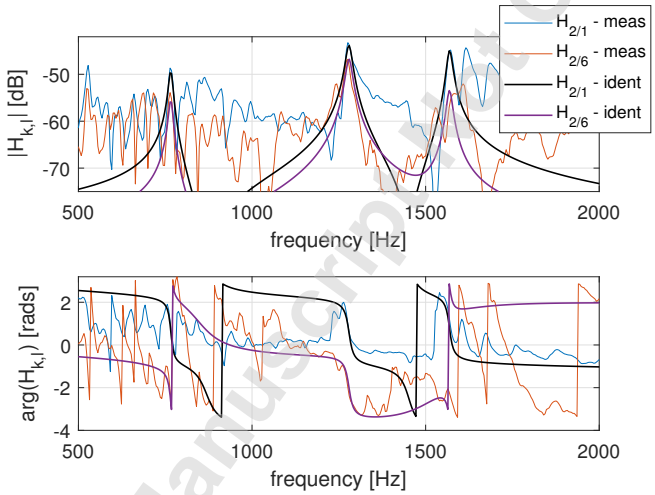

Fig. 9: Identification : FRF's of PZT n°2 to actuation (PZT 1 and 6), measurements and identifications from (1).

with a 2^{nd} order high pass filter:

$$F^{1/2}(s) = I_{N_s} \times k_F \times \left(\frac{2\xi_f \omega_1^2}{s^2 + 2s\xi_f \omega_1^2 + \omega_1^2} + \frac{2\xi_f \omega_2^2}{s^2 + 2s\xi_f \omega_2^2 + \omega_2^2} + \frac{2\xi_f \omega_3^2}{s^2 + 2s\xi_f \omega_3^2 + \omega_3^2} \right) \times \frac{s^2/\omega_{HP}^2}{1 + s^2/\omega_{HP}^2 + s/(Q_f \omega_{HP})} \quad (55)$$

Journal of Vibration and Acoustics. Received June 30, 2021;
Accepted manuscript posted December 21, 2021. doi:10.1115/1.4053358

Mode	$\omega_i/(2\pi)\ [Hz]$	ξ_i
1	770	7.5×10^{-3}
2	1282	5.0×10^{-3}
3	1576	4.3×10^{-3}

$H_{2,1}$				
	Magnitude	Phase $[deg]$	$a_i^{2,1}$	$b_i^{2,1}$
1	1153	136	-0.827×10^3	0.1658
2	5484	140	-4.192×10^3	0.4389
3	5510	141	-4.269×10^3	0.3517
$H_{2,6}$				
	Magnitude	Phase $[deg]$	$a_i^{2,6}$	$b_i^{2,6}$
1	847	-54	0.500×10^3	-0.1412
2	3634	-30	3.134×10^3	-0.2284
3	2214	-129	-1.395×10^3	-0.1736
$H_{3,1}$				
	Magnitude	Phase $[deg]$	$a_i^{3,1}$	$b_i^{3,1}$
1	1965	-177	-1.961×10^3	-0.0237
2	5425	138	-4.020×10^3	0.4525
3	6763	138	-5.048×10^3	0.4546
$H_{3,6}$				
	Magnitude	Phase $[deg]$	$a_i^{3,6}$	$b_i^{3,6}$
1	2115	-29	1.847×10^3	-0.2127
2	4789	-17	4.579×10^3	-0.1740
3	1179	-59	0.605×10^3	-0.1022
$H_{5,1}$				
	Magnitude	Phase $[deg]$	$a_i^{5,1}$	$b_i^{5,1}$
1	1481	148	-1.253×10^3	0.1631
2	4640	155	-4.218×10^3	0.2398
3	4556	118	-2.130×10^3	0.4067
$H_{5,6}$				
	Magnitude	Phase $[deg]$	$a_i^{5,6}$	$b_i^{5,6}$
1	1459	33	1.221×10^3	0.1649
2	4238	-20	3.990×10^3	-0.1774
3	1897	-75	0.495×10^3	-0.1849

Table 1: Identified modal parameters from the 3 PZT sensors FRF's to actuation.

with $k_F = 1.5 \times 10^2$, $\omega_{HP} = \omega_1$, $\xi_f = 7 \times 10^{-3}$, and $Q_f = 1$. The filters FRF's are shown in Figure 12. For the sake of simplicity, the control gain k_F appears only within the filter $F^{1/2}$ and is determined experimentally to avoid any instability of the linear closed-loop.

For the definition of $\bar{u}_{lin}$, the matrix P is defined as $P = I_2 \times 6.10^{-5}$ such that the norm of $S\tilde{A}$ and ΦS are approximately equivalent, balancing both performance and robustness for the linear control part.

Then, the Kalman observer of the initial system states x in (53) is computed considering the following co-variance matrices for process noise and measurement noise respectively: $V_d = I_{2nN_a}$ and $V_n = I_{N_s}$. The theoretical poles of the uncontrolled system and the SM-linear controlled system together with the observer poles are displayed in Figure

Journal of Vibration and Acoustics. Received June 30, 2021;
Accepted manuscript posted December 21, 2021. doi:10.1115/1.4053358

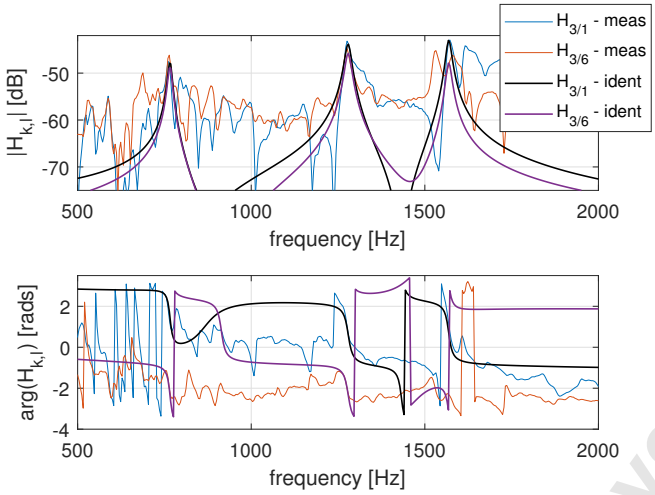

Fig. 10: Identification : FRF's of PZT n°3 to actuation (PZT 1 and 6), measurements and identifications from (1).

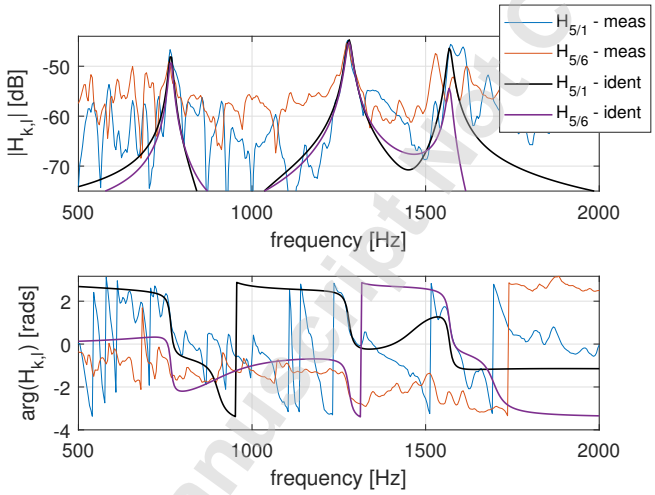

Fig. 11: Identification : FRF's of PZT n°5 to actuation (PZT 1 and 6), measurements and identifications from (1).

13.

Finally, the switching part of the control u_{nl} is tuned using $\rho = 1V$ and $\epsilon = 1.10^{-20}$.

4.4 Robustness study

As the system presents a very bad signal-to-noise ratio, one needs to study the induced lack of robustness due to bad system identification and the associated errors introduced in the synthesis strategy. As shown in Figure 7, the system dynamics are poorly observable and one needs to take into consideration this particularity that often occurs in real applications. In this subsection, the robustness of the proposed approach is investigated with two study cases on the simulated system response. First, parametric uncertainties are introduced in the identification process for the

Journal of Vibration and Acoustics. Received June 30, 2021;
Accepted manuscript posted December 21, 2021. doi:10.1115/1.4053358

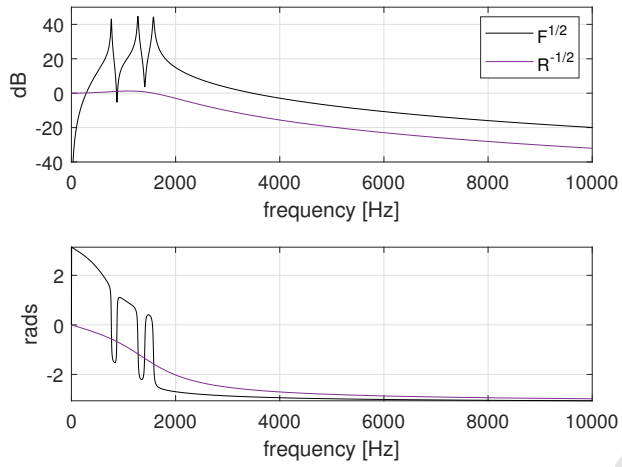

Fig. 12: FRF of the designed pre- and post-filters $F^{1/2}$ and $R^{-1/2}$.

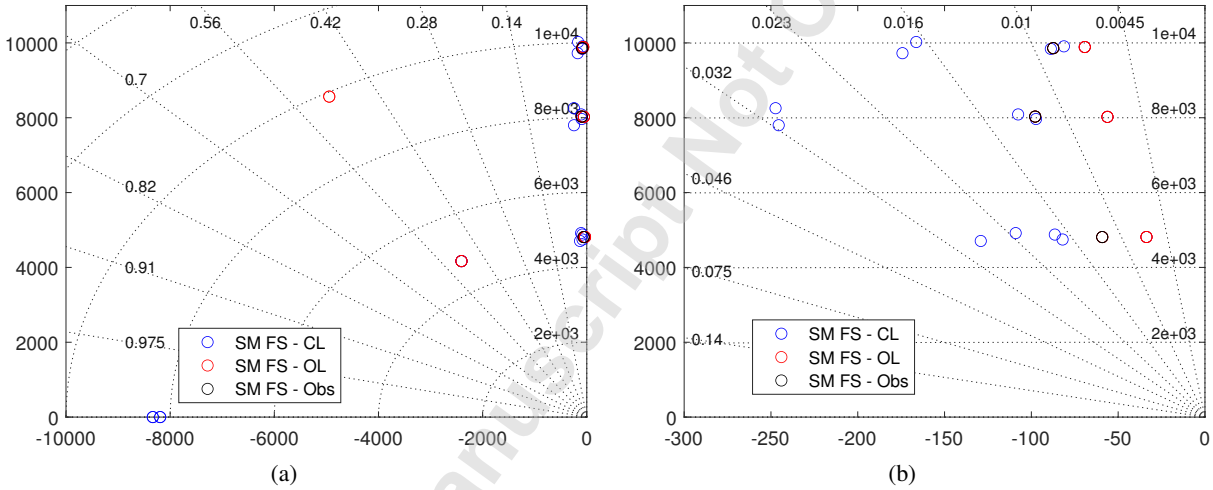

Fig. 13: Poles locations: controlled system, uncontrolled system and observer for the linear system (a) global view and (b) zoom close to imaginary axis.

observer computation to analyze the effects on the control performance. Then, the linear part of the closed-loop is defined unstable on purpose to observe the stabilizing contribution of the switching control part.

4.4.1 Robustness to modal phase identification uncertainties

The Figures 7 to 11 illustrate the complexity of identifying predominant modes in the PZT's voltage response. Thus, the measured FRF's frequency content is very dense and complex, augmenting the difficulty of determining precise modal parameters. Among all the identified parameters, the most critical ones are certainly the modal phases $\phi_i^{k,l}$ since damping is low and phase changes can be very steep.

Journal of Vibration and Acoustics. Received June 30, 2021;
Accepted manuscript posted December 21, 2021. doi:10.1115/1.4053358

To illustrate the robustness of the proposed identification and control method, the closed-loop system is simulated with Matlab/Simulink, using the measured time response of the PZT sensors to a known excitation signal. Besides, the transfer function matrix between actuators and sensors is considered ideal and is mathematically described as the system G in (16).

Thus, the simulations are performed using the proposed controller with a mistuned observer. Two types of errors are willingly introduced within the identified modal parameters: the first one is an identified modal phase deterministic error on the parameters $\phi_i^{k,l}$ from $-\pi/2$ to $\pi/2$ introduced on each mode separately. The second error type is an identified modal phase random error from $-\pi/2$ to $\pi/2$ introduced on each mode simultaneously and independently such that the phase error differs from one mode to another. Thus, the simulated modal phase identification errors are directly present in the observation matrix C, with the coefficients $a_i^{k,l}$ and $b_i^{k,l}$ for the computation of the mistuned observer gain matrix L.

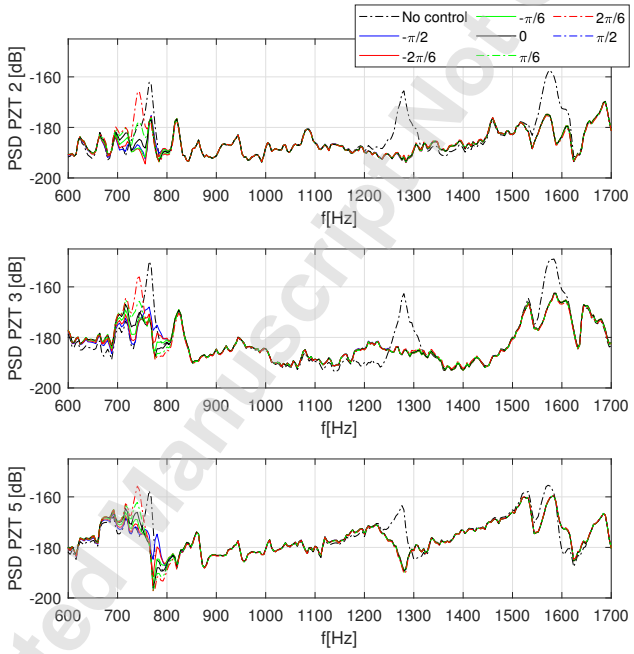

Fig. 14: Simulated power spectral density of the PZT sensors 2, 3, and 5 with an identified modal phase error from $-\pi/2$ to $\pi/2$ on the 1^{st} controlled mode.

The results in terms of sensors PSD response for the first error type are displayed in the Figures 14, 15 and 16 where the identified modal phase errors are introduced respectively for the first, second and third controlled mode.

First, one can observe that the control robustness is not equal depending on the considered mode. Re-injection of vibration energy, known as the spillover effect, is visible around the first and second one when the modal phase is

Journal of Vibration and Acoustics. Received June 30, 2021;
Accepted manuscript posted December 21, 2021. doi:10.1115/1.4053358

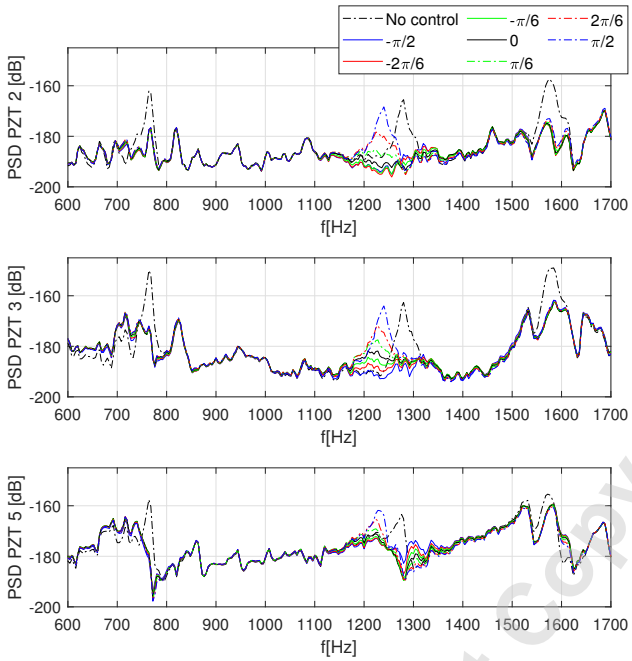

Fig. 15: Simulated power spectral density of the PZT sensors 2, 3, and 5 with an identified modal phase error from $-\pi/2$ to $\pi/2$ on the 2^{nd} controlled mode.

overestimated, or the observer being in advance with respect to the actual modal states. However, the third considered mode shows a more limited effect to modal phase identification errors. On the other hand, it is important to highlight that the closed-loop remains stable. Besides, the re-injection level does not exceed the original vibration level of the targeted mode, confirming the proposed approach robustness.

Then, in Figure 17 are presented the results for the second error type where random modal phase errors are introduced on all modes. Observing the effect of these parametric uncertainties on the simulated sensors response PSD, the conclusions drawn from the first error type are confirmed. Spillover may occur around the first and second mode, but the system still maintains stability.

4.4.2 Robustness to unstable linear closed-loop

Now, the linear part of the control is mistuned on purpose to introduce an unstable pole in the closed-loop. In practice, the linear gain matrix (39) can be partitioned as:

$$(S\tilde{B})^{-1}\left(S\tilde{A}-\Phi S\right)\hat{z}= \\ [K_{\hat{x}}\ \ K_F\ \ K_R]\ \ \left[\hat{x}^T\ \ x_F^T\ \ x_R^T\right]^T \tag{56}$$

Journal of Vibration and Acoustics. Received June 30, 2021;
Accepted manuscript posted December 21, 2021. doi:10.1115/1.4053358

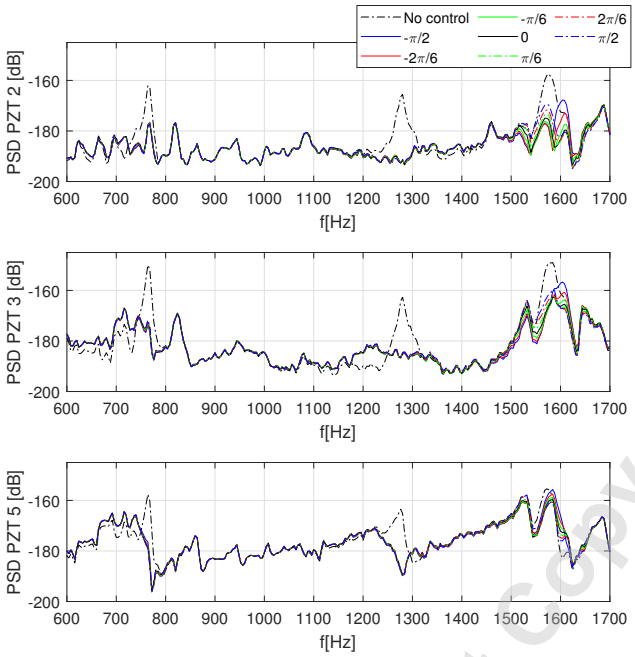

Fig. 16: Simulated power spectral density of the PZT sensors 2, 3, and 5 with an identified modal phase error from $-\pi/2$ to $\pi/2$ on the 3^{rd} controlled mode.

Then, the computed matrix K_F related to the states of the filter $F^{1/2}(s)$ is multiplied by a factor 10 such that two conjugate poles of the closed-loop $\tilde{A} - \tilde{B}\left[K_{\hat{x}} \;\; K_F \;\; K_R\right]$ travel from the LHP to the unstable RHP as:

$$MAX\left(Re\left\{\lambda_i\left\{\tilde{A} - \tilde{B}\left[K_{\hat{x}} \;\; K_F \;\; K_R\right]\right\}\right\}\right) = 4.9 \tag{57}$$

with associated negative damping of -0.12%. In practice, such bad tuning of the controller can perfectly happen since the identification is subject to many parametric uncertainties on complex smart structures as mentioned earlier.

The resulting unstable controller is then simulated as in the previous study. At start, no control is applied from $t = 0$ to $t_1 = 3s$. In a second time, from $t_1 = 3s$ to $t_2 = 4s$, only the unstable linear control is applied to initiate a diverging behavior in the closed-loop. Finally, at $t > t_2$, the nonlinear switching control part is applied.

The time-domain results on the two terms of the sliding vector σ are displayed in Figure 18. One can easily notice the divergence of the closed-loop at $t = t_1$ due to the unstable poles. However, from $t = t_2$ to the end of the simulation, the switching control is applied and stabilizes the unstable closed-loop. Thus, the sliding vector quickly converges to a stable vicinity of the sliding manifold.

Journal of Vibration and Acoustics. Received June 30, 2021;
Accepted manuscript posted December 21, 2021. doi:10.1115/1.4053358

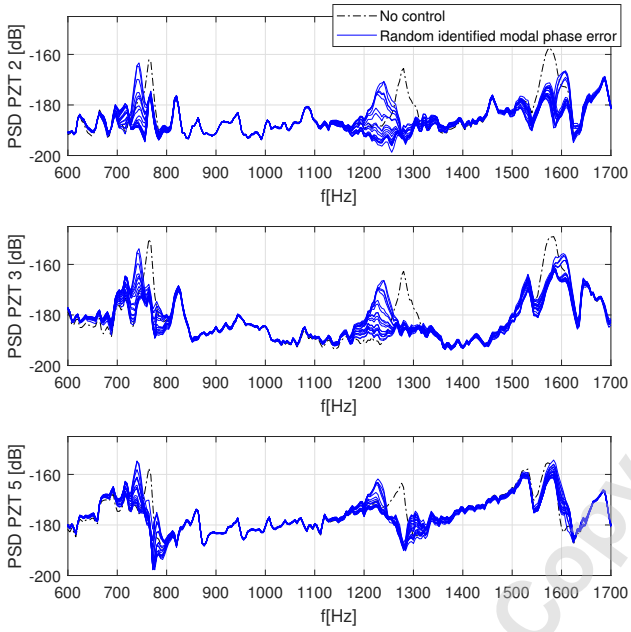

Fig. 17: Simulated power spectral density of the PZT sensors 2, 3, and 5 with an identified modal phase random error from $-\pi/2$ to $\pi/2$ on all modes.

To support this result, the simulated PSD responses of the PZT sensors are shown in Figure 19 without control and with the SMC. Even if the control performance is degraded due to the destabilizing linear part, causing a lot of spillover phenomena around the target modes, the closed-loop is forced to maintain within the stability domain. Furthermore, the target modes are still somehow controlled as it can be observed on the different sensors PSD. Finally, in terms of control cost, the simulated voltage RMS values for the destabilized controller on both actuators are respectively 2 and 2.6 times higher than the nominal controller.

Finally, considering critical parametric uncertainties such as errors on the identified modal phases or badly tuned controllers causing unstable linear closed-loop, the proposed identification and control method is robust. A limited effect of the perturbations on the control performance is guaranteed or at least, the closed-loop stability is maintained. This observation is crucial to support the relevance of the proposed approach when applied to complex smart composite structures.

4.5 Experimental control results

This subsection now presents the experimental results obtained on the real smart composite spoiler with the proposed controller. The perturbation signal applied to PZT 4 is a white noise of maximum amplitude 3V and sampling frequency 20kHz.

The main results are presented in Figure 20 which shows the power spectral densities of the PZT sensors 2,3, and

Journal of Vibration and Acoustics. Received June 30, 2021;
Accepted manuscript posted December 21, 2021. doi:10.1115/1.4053358

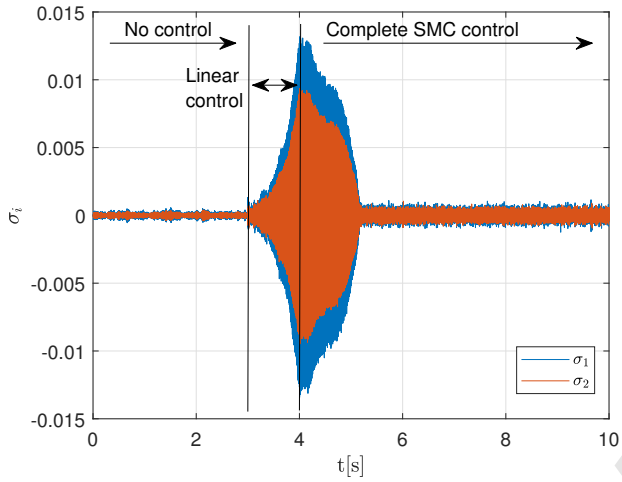

Fig. 18: Simulated system time response to unstable linear control, terms of the sliding vector σ with no control, unstable linear control only and complete SMC control.

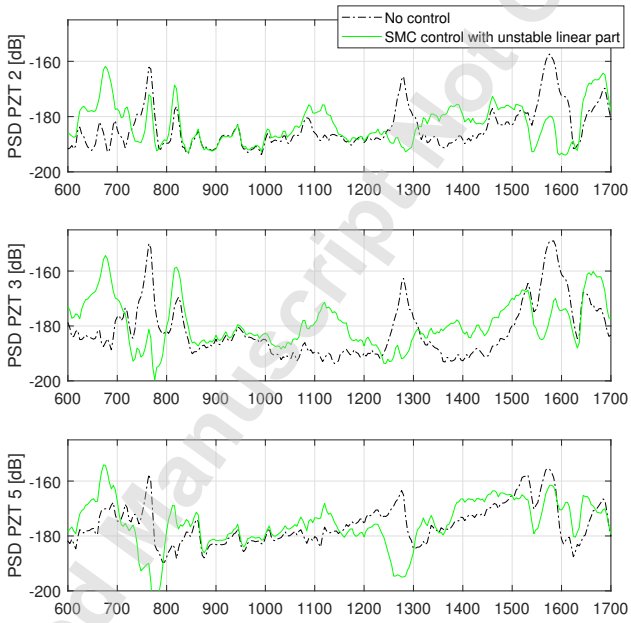

Fig. 19: Simulated power spectral density of the PZT sensors 2, 3, and 5 with no control and SMC with unstable linear part.

5 without control, then only with the linear part of the control or only the nonlinear part and finally the complete SMC.

300 Firstly, one can notice that the measured voltage level, image of the PZT strain, of the 3 targeted modes: 770Hz, 1282Hz, and 1576Hz is significantly reduced, whether using the linear control or the switching control. Yet, both parts are complementary considering the control performance and robustness.

For instance, the linear control tends to increase the vibration level above 1600Hz (3^{rd} controlled mode) on all

Journal of Vibration and Acoustics. Received June 30, 2021;
Accepted manuscript posted December 21, 2021. doi:10.1115/1.4053358

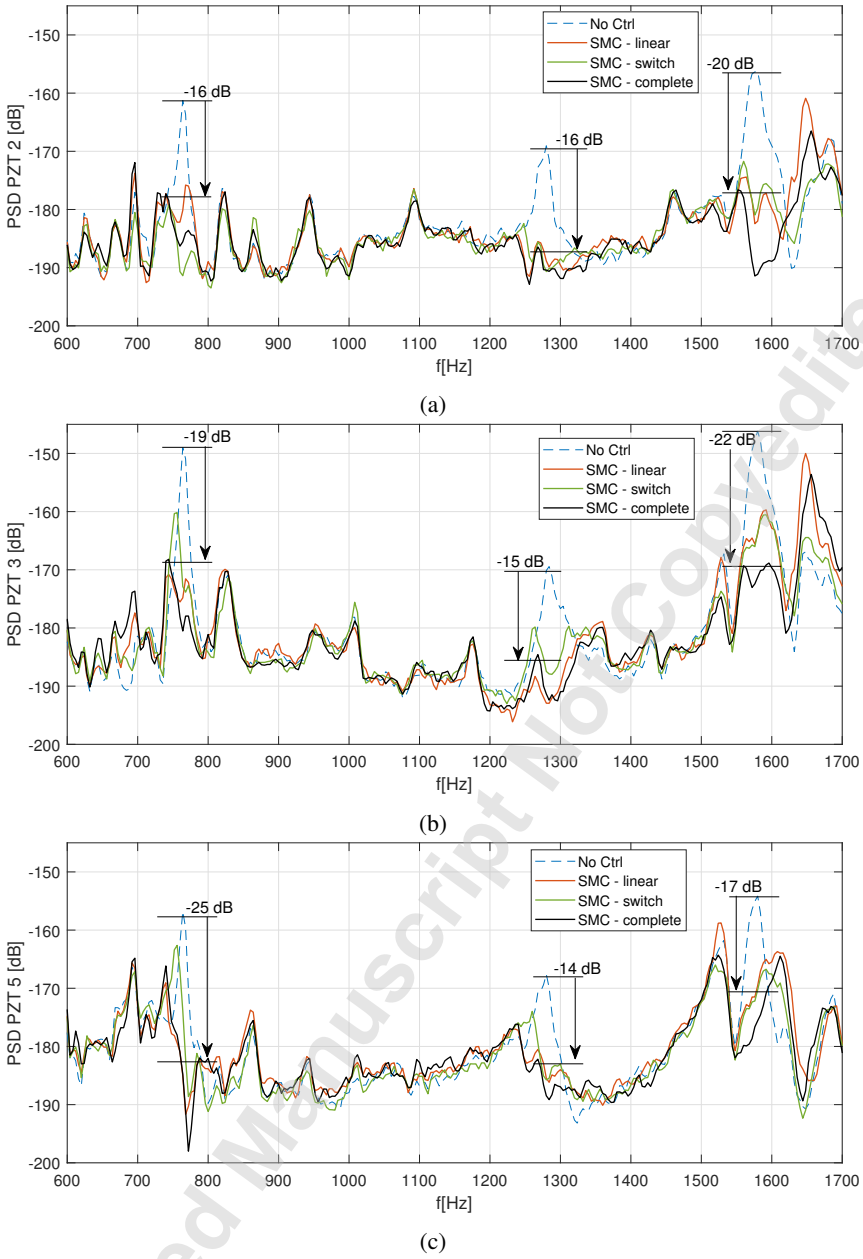

Fig. 20: Experimental results - power spectral density of the PZT sensors (a) PZT 2, (b) PZT 3, (c) PZT 5 without control, with only the linear control u_{lin}, only the switching control u_{nl}, and the complete SMC controller.

PZT sensors due to the spillover phenomenon from the simplified identification process. However, the nonlinear control displays more robustness to parametric uncertainties between the model and the real system considering the aforementioned bandwidth above the 3^{rd} mode.

On the other hand, the linear control causes a much better attenuation for the 1^{st} mode on PZT 3 and 5 than the switching control.

Journal of Vibration and Acoustics. Received June 30, 2021;
Accepted manuscript posted December 21, 2021. doi:10.1115/1.4053358

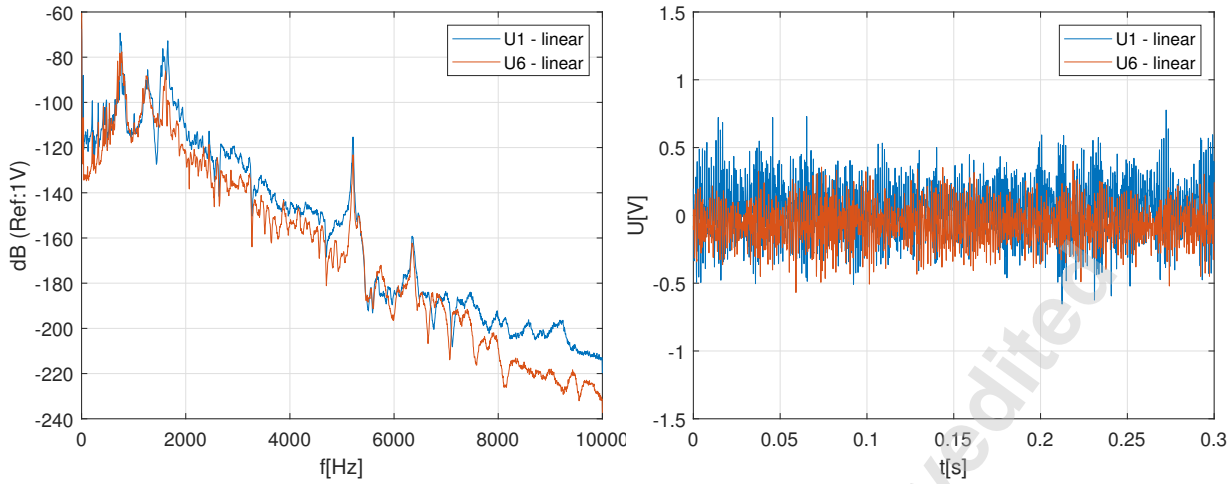

(a) (b)

Fig. 21: Experimental results - (a) Power spectral density of the linear control voltages u_{lin} and (b) time signals for 0.3s.

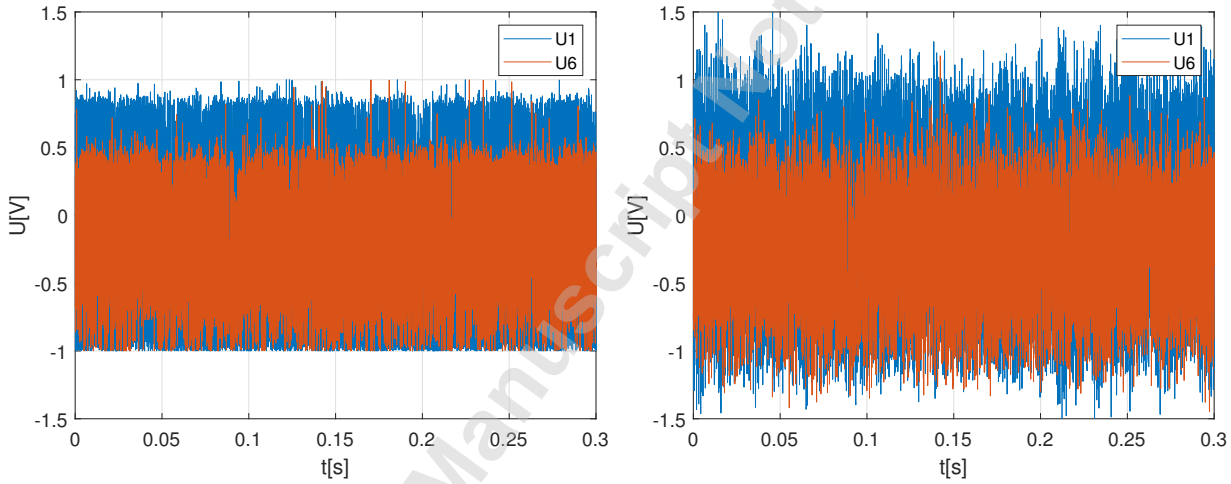

(a) (b)

Fig. 22: Experimental results - time signals for (a) the switching control part u_{nl} and (b) the total control $u_{nl} + u_{lin}$ for 0.3s.

Thus, by combining both parts of the control and applying the complete SMC to the smart composite structure as presented originally in 2, the attenuation level of the considered modes is very interesting, going from -14dB on the 2^{nd} mode for PZT 5 to -22dB on the 1^{st} mode for PZT 5.

Remark It is worth noticing that since the observer is very simplified considering only three selected modes in comparison to the complex modal content of the real structure response, the measurement y is to be considered by the controller as largely noisy. However, the results in terms of control performance on the real composite smart

structure confirm again the robustness of the proposed approach and its ability to compensate for noisy measurements and highly uncertain systems.

To have a more in-depth view of the proposed vibration control method energy cost, the Figure 21 shows the power spectral densities and time-domain extracts of the linear control signals for PZT actuators 1 and 6. As expected, the proposed modal-shaped SMC makes the control focus on the targeted modes and avoids unnecessary frequency content in the control signal.

Finally, Figure 22 displays time-domain extracts of the switching control part and the total control signals of the SMC to highlight the main energy cost for such vibration attenuation. One can notice first that due to real time computation limitations, the mathematical formulation of the unit vector in (43), and the parameter ϵ, the expression $P\sigma/(||P\sigma|| + \epsilon)$ is not a pure switching function.

Table 2 finally displays the voltage RMS values for the excitation signal applied to the PZT 4 with the linear, switching, and total control signals applied to PZT actuators 1 and 6. Thus, the voltage RMS value of the nonlinear part is approximately 4 times superior to the linear one, showing that the resulting control performance still comes with power cost.

Hence, SMC control associated with a modal-shaped switching function provides both better performance and robustness than the linear part only. However, relay nonlinearities in the closed-loop might not be a desirable strategy for all vibrating structures depending especially on the actuators technology, bandwidth, and power electronics.

	Voltage RMS value
Excitation - U_4	1.34
$U_{1,lin}$	0.2
$U_{6,lin}$	0.16
$U_{1,nl}$	0.83
$U_{6,nl}$	0.54
$U_{1,tot}$	0.84
$U_{6,tot}$	0.59

Table 2: RMS voltage values for excitation signal, linear control signals, switching control signals and total control signals.

5 CONCLUSION

This paper proposed a complete active modal vibration control method based on a sliding mode controller applied to a smart composite spoiler-shaped structure with integrated PZT transducers as actuators and sensors within the glass fiber layers. The first step has been the mechanical-electrical coupled system identification with a modal reduced

model. Then, based on filtered states, a modal-shaped switching function has been designed using a general formulation allowing control of multiple selected vibration modes on multiple sensors with multiple actuators. The stability of the linear and nonlinear switching parts of the controller has been addressed. Thus, the controller was successfully applied to the representative smart composite structure. The experimental results obtained comparing the linear part of the control with the nonlinear part and finally, the complete SMC confirm the relevance of switching control methods for modal vibration control. The level of performance achieved with the total control signal for each actuator went from $-14dB$ to $-22dB$ on three different controlled modes and each PZT in-loop sensor. Finally, robustness is a key property for the control of real complex smart structures. The proposed identification and control approach demonstrated to provide such robustness to parametric or identification uncertainties, noise, and badly tuned controllers. In conclusion, SMC methods are rarely used for active vibration control since they are nonlinear by essence. However, the controller design in this manuscript illustrates their performance and also robustness for modal control of complex smart structures with rich frequency response content and uncertainties on the identification.

ACKNOWLEDGEMENTS

The authors would like to thank Institut Carnot for supporting the project and providing the funding for this research.

REFERENCES

[1] Tuloup, C., Harizi, W., Aboura, Z., Meyer, Y., Khellil, K., & Lachat, R. (2019). On the use of in-situ piezoelectric sensors for the manufacturing and structural health monitoring of polymer-matrix composites: A literature review. Composite Structures, 215, 127-149. https://doi.org/10.1016/j.compstruct.2019.02.046

[2] Shivashankar, P., & Gopalakrishnan, S. (2020). Review on the use of piezoelectric materials for active vibration, noise, and flow control. Smart Materials and Structures, 29(5), 053001. https://doi.org/10.1088/1361-665X/ab7541

[3] Safaei, M., Sodano, H. A., & Anton, S. R. (2019). A review of energy harvesting using piezoelectric materials: state-of-the-art a decade later (2008–2018). Smart Materials and Structures, 28(11), 113001. https://doi.org/10.1088/1361-665X/ab36e4

[4] Chomette, B., Remond, D., Chesne, S., & Gaudiller, L. (2008). Semi-adaptive modal control of on-board electronic boards using an identification method. Smart Materials and Structures, 17(6), 065019. https://doi.org/10.1088/0964-1726/17/6/065019

[5] Preumont, A. (2018). Vibration control of active structures: an introduction (Vol. 246). Springer.

[6] Zhang, W., Qiu, J., & Tani, J. (2004). Robust vibration control of a plate using self-sensing actuators of piezoelectric patches. Journal of intelligent material systems and structures, 15(12), 923-931. https://doi.org/10.1177/1045389X04045153

[7] Shtessel, Y., Edwards, C., Fridman, L., & Levant, A. (2014). Sliding mode control and observation (Vol. 10). New York, NY: Springer New York.

[8] Sung, K. G., Han, Y. M., Cho, J. W., & Choi, S. B. (2008). Vibration control of vehicle ER suspension system using fuzzy moving sliding mode controller. Journal of Sound and Vibration, 311(3-5), 1004-1019. https://doi.org/10.1016/j.jsv.2007.09.049

[9] Ning, D., Sun, S., Wei, L., Zhang, B., Du, H., & Li, W. (2017). Vibration reduction of seat suspension using observer based terminal sliding mode control with acceleration data fusion. Mechatronics, 44, 71-83. https://doi.org/10.1016/j.mechatronics.2017.04.012

[10] Mien, V., Tu, P. H. T., Nguyen, N. P., & Choi, S. B. (2020). A new optimal sliding mode controller with adjustable gains based on Bolza-Meyer criterion for vibration control. Journal of Sound and Vibration, 485, 115542. https://doi.org/10.1016/j.jsv.2020.115542

[11] Nguyen, S. D., Lam, B. D., & Choi, S. B. (2021). Smart dampers-based vibration control–Part 2: Fractional-order sliding control for vehicle suspension system. Mechanical Systems and Signal Processing, 148, 107145. https://doi.org/10.1016/j.ymssp.2020.107145

[12] Hu, Q., & Friswell, M. I. (2008). Adaptive sliding mode attitude and vibration control of flexible spacecraft under unknown disturbance and uncertainty. IFAC Proceedings Volumes, 41(2), 9871-9876. Seoul, Korea, July 6-11, 2008. https://doi.org/10.3182/20080706-5-KR-1001.01670

[13] Concha, A., Thenozhi, S., Betancourt, R. J., & Gadi, S. K. (2021). A tuning algorithm for a sliding mode controller of buildings with ATMD. Mechanical Systems and Signal Processing, 154, 107539. https://doi.org/10.1016/j.ymssp.2020.107539

[14] David Young, K., & Özgüner, Ü. (1993). Frequency shaping compensator design for sliding mode. International Journal of Control, 57(5), 1005-1019. https://doi.org/10.1080/00207179308934427

[15] Nonami, K., Nishimura, H., & Tian, H. (1996). $H\infty/\mu$ control-based frequency-shaped sliding mode control for flexible structures. JSME international journal. Ser. C, Dynamics, control, robotics, design and manufacturing, 39(3), 493-501 https://doi.org/10.1299/jsmec1993.39.493

[16] Yanada, H., & Ohnishi, H. (1999). Frequency-shaped sliding mode control of an electrohydraulic servo-motor. Proceedings of the Institution of Mechanical Engineers, Part I: Journal of Systems and Control Engineering, 213(6), 441-448. https://doi.org/10.1243/0959651991540269

[17] Acarman, T., & Özgüner, Ü. (2002). Frequency shaping compensation for backstepping sliding mode control. IFAC Proceedings Volumes, 35(1), 37-42. 15th Triennial World Congress, Barcelona, Spain. https://doi.org/10.3182/20020721-6-ES-1901.01077

[18] Royel, S., Ha, Q. P., & Aguilera, R. P. (2018, November). Frequency-Shaped Second-Order Sliding Mode Control for Smart Suspension Systems. In 2018 15th International Conference on Control, Automation, Robotics and Vision (ICARCV) (pp. 907-912). IEEE. 18-21 Nov. 2018, Singapore. DOI:10.1109/ICARCV.2018.8581139

[19] Zuo, L., & Slotine, J. J. E. (2005). Robust vibration isolation via frequency-shaped sliding control and modal decomposition. Journal of Sound and Vibration, 285(4-5), 1123-1149. https://doi.org/10.1016/j.jsv.2004.09.014

[20] Qiu, Z. C., Zhang, X. M., Wang, Y. C., & Wu, Z. W. (2009). Active vibration control of a flexible beam using a non-collocated acceleration sensor and piezoelectric patch actuator. Journal of sound and vibration, 326(3-5), 438-455. https://doi.org/10.1016/j.jsv.2009.05.034

[21] Zhang, Q., Li, C., Zhang, J., & Zhang, J. (2017). Smooth adaptive sliding mode vibration control of a flexible parallel manipulator with multiple smart linkages in modal space. Journal of Sound and Vibration, 411, 1-19. https://doi.org/10.1016/j.jsv.2017.08.052

[22] Oveisi, A., & Nestorović, T. (2016). Robust observer-based adaptive fuzzy sliding mode controller. Mechanical Systems and Signal Processing, 76, 58-71. https://doi.org/10.1016/j.ymssp.2016.01.015

[23] Wang, R. L., Gu, H., & Song, G. (2014). Adaptive robust sliding mode vibration control of a flexible beam using piezoceramic sensor and actuator: an experimental study. Mathematical problems in engineering, 2014. https://doi.org/10.1155/2014/606817

[24] Fang, Y., Fei, J., & Hu, T. (2018). Adaptive backstepping fuzzy sliding mode vibration control of flexible structure. Journal of Low Frequency Noise, Vibration and Active Control, 37(4), 1079-1096. https://doi.org/10.1177/1461348418767097

[25] Rahmani, B. (2018). Adaptive fuzzy sliding mode control for vibration suppression of a rotating carbon nanotube-reinforced composite beam. Journal of Vibration and Control, 24(12), 2447-2463. https://doi.org/10.1177/1077546316687937

[26] Hu, J., & Zhu, D. (2012). Vibration Control of Smart Structure Using Sliding Mode Control with Observer. Journal of Computers., 7(2), 411-418. DOI:10.4304/jcp.7.2.411-418

[27] Duc, G., & Mammar, S. (1992). Frequency-Shaped LQG/LTR Design: Application to the Robust Stabilization of an Helicopter. In Design Methods of Control Systems (pp. 39-44). Pergamon. https://doi.org/10.1016/B978-0-08-041902-2.50011-8

[28] Young, P., & Jakeman, A. (1980). Refined instrumental variable methods of recursive time-series analysis Part

III. Extensions. International Journal of Control, 31(4), 741-764. https://doi.org/10.1080/00207178008961080

[29] Garnier, H., Mensler, M., & Richard, A. (2003). Continuous-time model identification from sampled data: implementation issues and performance evaluation. International journal of Control, 76(13), 1337-1357. https://doi.org/10.1080/0020717031000149636

[30] Chesné, S., Jean-Mistral, C., & Gaudiller, L. (2013). Experimental identification of smart material coupling effects in composite structures. Smart materials and structures, 22(7), 075007. https://doi.org/10.1088/0964-1726/22/7/075007

[31] Laub, A., Heath, M., Paige, C., & Ward, R. (1987). Computation of system balancing transformations and other applications of simultaneous diagonalization algorithms. IEEE Transactions on Automatic Control, 32(2), 115-122. DOI:10.1109/TAC.1987.1104549

[32] Liao, X., & Yu, P. (2008). Absolute stability of nonlinear control systems (Vol. 25). Springer Science & Business Media.

LIST OF FIGURES

LIST OF TABLES